PAPER Special Section on Analog Circuits and Related SoC Integration Technologies

EMI Camera LSI (EMcam) with On-Chip Loop Antenna Matrix to Measure EMI Noise Spectrum and Distribution

Naoki MASUNAGA[†*], **Koichi ISHIDA**[††a)], ***Members***, **Takayasu SAKURAI**[††], ***Fellow***, ***and*** **Makoto TAKAMIYA**[†††], ***Member***

SUMMARY This paper presents a new type of electromagnetic interference (EMI) measurement system. An EMI Camera LSI (EMcam) with a 12×4 on-chip $250 \times 50\,\mu m^2$ loop antenna matrix in 65 nm CMOS is developed. EMcam achieves both the 2D electric scanning and 60 μm-level spatial precision. The down-conversion architecture increases the bandwidth of EMcam and enables the measurement of EMI spectrum up to 3.3 GHz. The shared IF-block scheme is proposed to relax both the increase of power and area penalty, which are inherent issues of the matrix measurement. The power and the area are reduced by 74% and 73%, respectively. EMI measurement with the smallest $32 \times 12\,\mu m^2$ antenna to date is also demonstrated.

key words: *electromagnetic interference, on-chip loop antenna, down-conversion, noise distribution*

1. Introduction

Electromagnetic interference (EMI) that degrades the dependability of electronic equipments is becoming a serious issue. Electromagnetic compatibility (EMC) at the LSI level has been important, because LSIs are often the main noise source in electronic equipments [1]. In particular, intrasystem EMC problem in small electronic equipments such as cell-phones is concerned because of (1) the increasing density of the packaging, (2) the increasing number of various RF transceivers within a electronic device, and (3) the increasing signal frequency higher than 1 GHz, which result in the downsizing of the EMI antenna. In order to measure the EMI noise generated from the fine pattern on PCB or the on-chip interconnect, 2D EMI distribution measurement with 60 μm-level spatial precision, which is finer than typical PCB design rule, is required.

Figure 1 shows dimensions and spatial resolution of recent EMI measurement systems [2]–[8]. To efficiently and accurately measure the 2D EMI distribution, the electric scanning instead of the conventional mechanical scanning of the EMI probe [2] is required. All the conventional measurement method, however, do not satisfy both the 2D electric scanning and the 60 μm precision. The spatial precision of the conventional 2D electric scanning [3]–[5] is more than 7.5 mm. Though the smallest EMI probe with $50 \times 22\,\mu m^2$ is reported [7], the probe is single and used for the mechanical scanning.

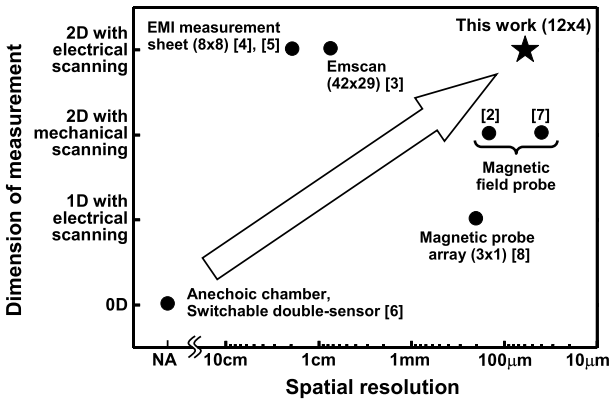

Fig. 1 Dimension and spatial resolution of recent EMI measurement systems.

To solve the problem of the conventional EMI measurement methods, an EMI camera LSI (EMcam) with the matrix of on-chip loop antennas and measurement circuits is proposed. The feasibility of 2D EMI distribution measurement with 60 μm-level spatial precision is demonstrated by using the EMcam [9].

2. EMI Camera LSI (EMcam)

2.1 Overview of EMcam

Figure 2 shows an overview and benefits of the proposed EMcam. The EMcam chip consists of an EMI measurement circuit as shown in Fig. 3 and on-chip loop antennas. By putting the EMcam on top of the DUT LSI, the EMcam measures within-die 2D distributions of EMI noise at various frequencies. The EMcam can measure also the EMI noise distribution on a PCB in the same way. Both the location of the EMI noise source and its frequency can be measured simultaneously with 60 μm-level spatial precision.

2.2 Measurement Core Circuit and Operation

Figure 3 shows the block diagram of the measurement core circuit in the EMcam. The EMI noise is picked up by the on-chip loop antenna. Then the EMI noise is down-converted

Manuscript received October 18, 2011.
Manuscript revised January 26, 2012.

[†]The author was with the Institute of Industrial Science, The University of Tokyo, Tokyo, 153-8505 Japan.
[††]The authors are with Institute of Industrial Science, The University of Tokyo, Tokyo, 153-8505 Japan.
[†††]The author is with VLSI Design and Education Center, The University of Tokyo, Tokyo, 113-8654 Japan.
[*]Presently, with Terumo Corporation, Tokyo, 100-0005 Japan.
a) E-mail: ishida@iis.u-tokyo.ac.jp

DOI: 10.1587/transele.E95.C.1059

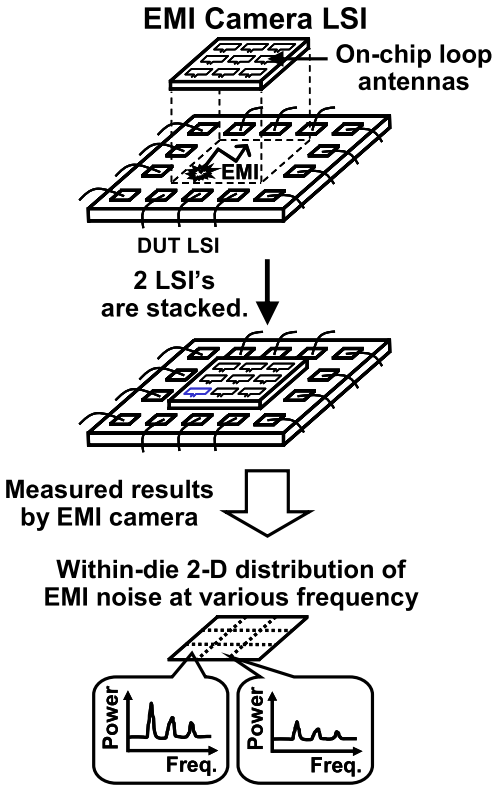

Fig. 2 Overview and benefits of the proposed EMcam (© 2010 IEEE).

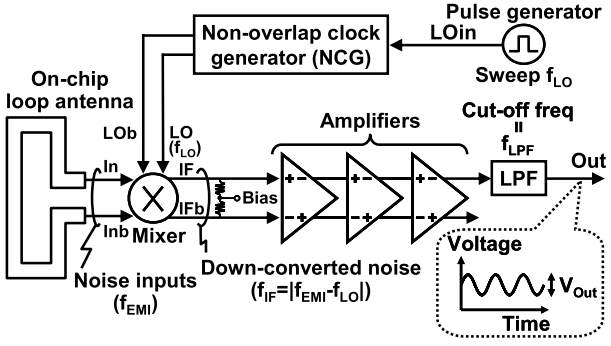

Fig. 3 Block diagram of measurement core circuit in EMcam (© 2010 IEEE).

by the mixer. The down-converted noise, f_{IF} is given by $f_{IF} = |f_{EMI} - f_{LO}|$, where f_{EMI} and f_{LO} are the frequencies of the EMI noise and the non-overlap clock generator (NCG), respectively. Then f_{IF} is amplified and filtered by LPF. While the noise inputs are simply amplified by high-bandwidth amplifiers in [8], the down-conversion is very important in our matrix measurement, because the down-converted noise can be handled with the low-bandwidth amplifiers that consume low power. That is, the total power consumption can be reduced with a high bandwidth up to 3.3 GHz for the EMI noise measurement.

Figures 4(a) and (b) show schematics of the mixer and the amplifiers in Fig. 3. The passive mixer is used to reduce the power consumption. To amplify differential voltage in-

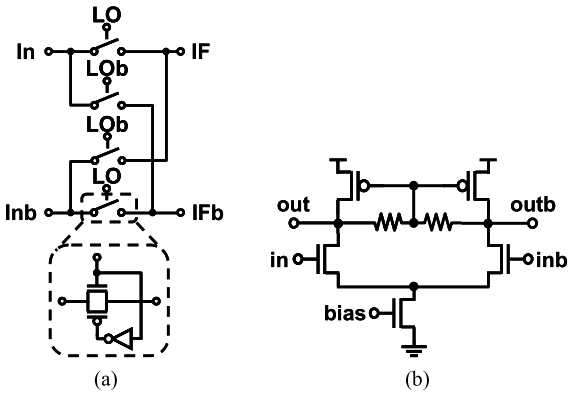

Fig. 4 Circuit schematics. (a) Mixer. (b) Amplifier (one stage) (© 2010 IEEE).

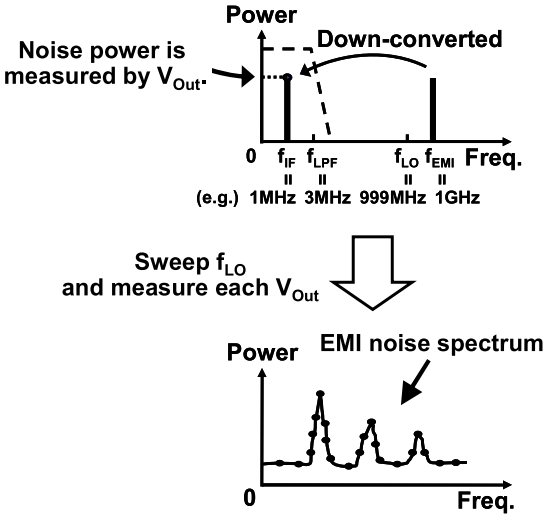

Fig. 5 Principle of EMI noise spectrum measurement using the circuit in Fig. 3. (© 2010 IEEE)

duced by RF magnetic field, the amplifier consists of three-stage fully-differential amplifiers with the common mode feedback by resistors suppressing RF electric field-induced voltages (Fig. 4(b) shows one stage for simplicity). The simulated open loop gain and the unity gain frequency of the amplifier are 16 dB and 6.2 GHz, respectively.

Figure 5 shows a procedure to obtain the EMI noise spectrum using the circuit in Fig. 3. For instance, when f_{EMI} is 1 GHz and f_{LO} is set at 999 MHz, f_{IF} is 1 MHz by the down-conversion. The noise power at 1 MHz can be measured by using LPF with the cut-off frequency of 3 MHz. By sweeping f_{LO} and measuring V_{Out} shown in Fig. 3 at each f_{LO} (e.g. f_{LO} is swept from 15 MHz to 3 GHz, 3 MHz step), the EMI noise spectrum is obtained.

2.3 Matrix Circuits for EMI Measurement

Figures 6(a) and (b) show schematics of a straightforward and the proposed matrix circuits in the EMcam, respectively. Although 12×4 antenna matrix circuits are implemented in our design, the schematics in Fig. 6 are drawn as 4×4

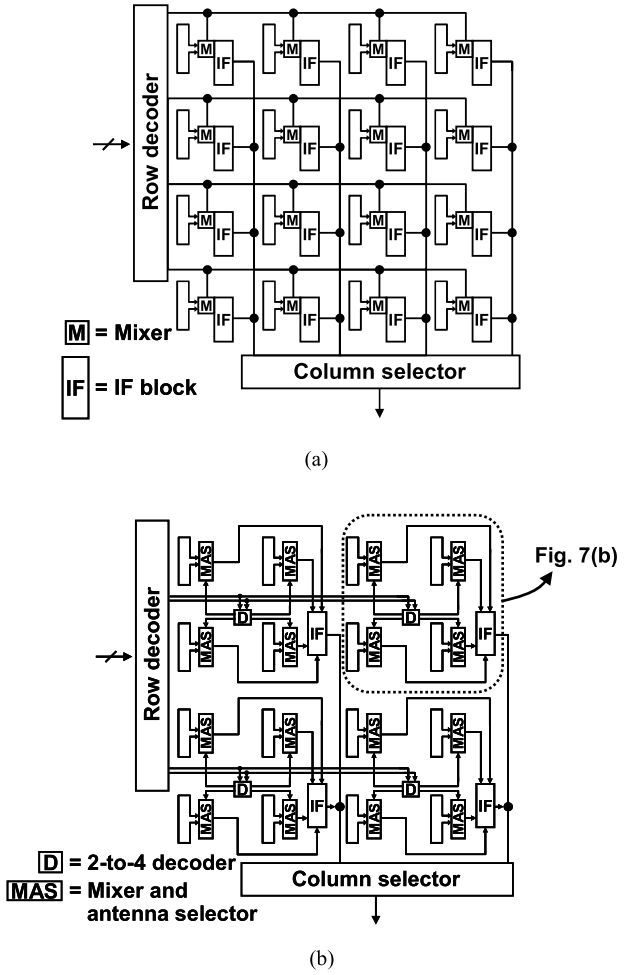

Fig. 6 Schematic of (a) straightforward and (b) proposed matrix circuits in EMcam (© 2010 IEEE).

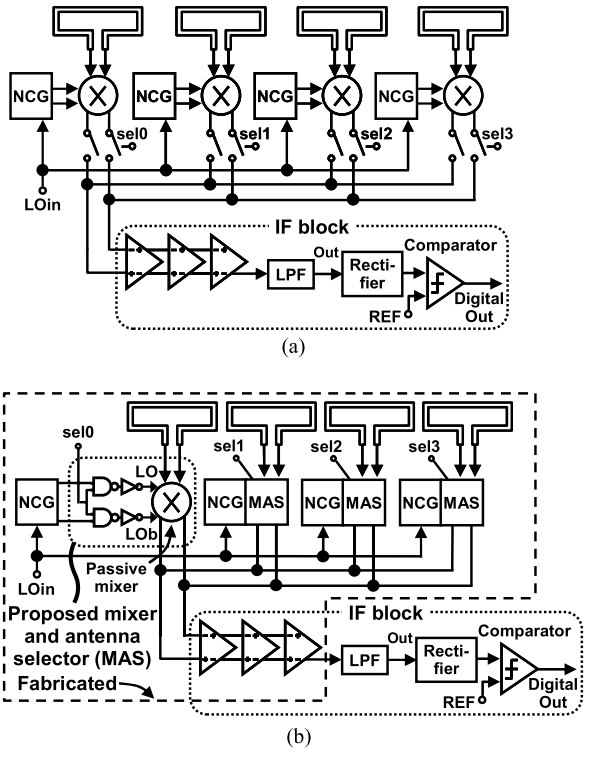

Fig. 7 Schematic of (a) straightforward and (b) proposed measurement circuit array in EMcam (© 2010 IEEE).

matrix circuits for simplicity. In order to relax both the increasing power and area penalty, which are inherent issues for the matrix measurement, the IF block is shared among 4 antennas, which is enabled by the proposed measurement circuit array. In the straightforward matrix circuits, each antenna has a mixer and a high-power IF block. In contrast, in the proposed matrix circuits, each antenna has the proposed 'mixer and antenna selector (MAS)' circuit, and 4 antennas share a decoder and the IF block. By sharing the high-power IF block, the power and the circuit area are reduced by 74% and 73%, respectively.

Figures 7(a) and (b) show schematics of the straightforward and proposed measurement circuit array in the EMcam, respectively. The circuit in Fig. 7(b) is a part of the proposed matrix in Fig. 6(b). The analog signal (Out) is converted to a digital signal by a rectifier and a comparator to efficiently get the measured outputs from the matrix. In the straightforward circuit array, there are series switches between the mixer and the IF block. Noise signals detected in the on-chip loop antenna are attenuated by the series switches and the sensitivity of the measurement circuit becomes lower. In contrast, in the proposed circuit array, each antenna has the NCG and MAS circuit. By controlling LO and LOb in MAS, MAS operates as the mixer or the antenna selector with small area and power overhead. When sel0 is high, MAS operates as the mixer. When sel0 is low, both LO and LOb are low, and the antenna is separated from the amplifiers. In this way, the proposed MAS can operate as both the mixer and antenna selector. Since the number of transistor switches in the signal path can be reduced, the sensitivity problem can be minimized. In addition, in MAS, only an antenna coil under measurement is connected to the amplifiers. Remaining neighbor antenna coils are left open. Therefore, mutual inductances between the coils can be negligible.

3. Measurement Results

3.1 EMcam Chip

The front-end block of the EMcam shown in Fig. 7(b) was fabricated with 1.2 V, 65 nm CMOS process. The chip micrographs and layouts are shown in Fig. 8. Figure 8(a) shows overall circuit of the EMcam chip. A 12×4 on-chip loop antenna matrix is embedded and the size of the antenna is $250 \times 50\,\mu\text{m}^2$. The antenna pitch is $260\,\mu$m and $60\,\mu$m in a horizontal and vertical direction, respectively. Figure 8(b) shows a layout of a measurement circuit in the EMcam. The core area of the MAS and NCG is $46\,\mu\text{m}^2$. In contrast, that of the amplifiers is $2130\,\mu\text{m}^2$; it is much larger than that of the MAS and NCG. Figure 8(c) shows the photomicrograph and layout of the standard antenna ($250 \times 50\,\mu\text{m}^2$).

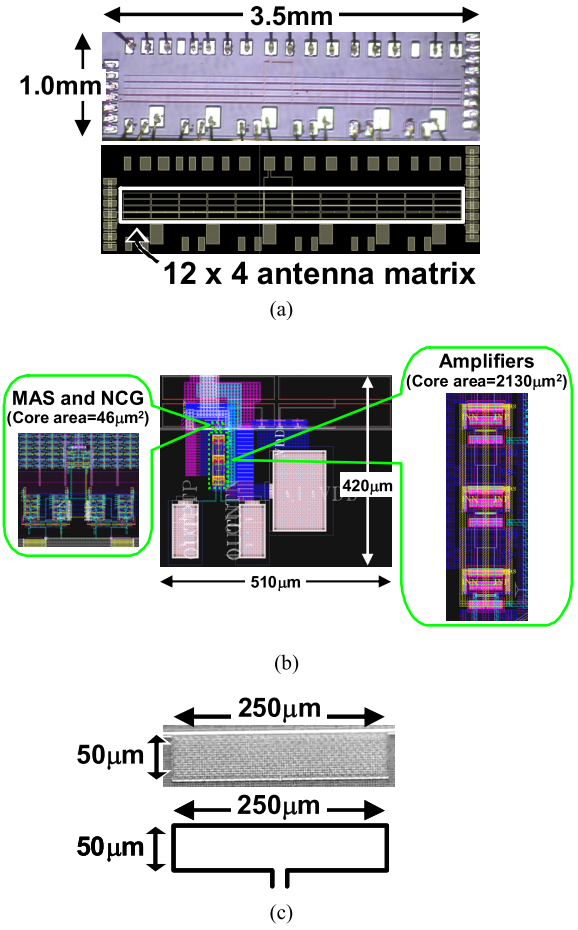

Fig. 8 Chip microphotographs and layouts. (a) Overall circuit of EMcam. (b) Measurement circuit in EMcam. (c) Antenna.

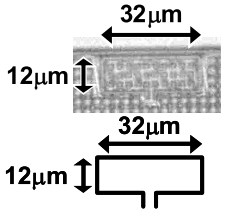

Fig. 9 Chip microphotograph and layout of smallest antenna.

In order to show the feasibility of the EMI noise measurement with higher-spatial resolution, the smallest size loop antenna ($32 \times 12\,\mu m^2$) is fabricated. Figure 9 shows the photomicrograph and layout of the smallest antenna.

3.2 Off-Chip DUT

Figure 10 shows the photograph of the measurement setup to verify the detection of the EMI noise by the off-chip DUT. The off-chip DUT is made with the center core of the thin coaxial cable and the other side is connected to an external 1 GHz signal generator that emulates the EMI noise.

Figures 11(a) and (b) show the output waveforms of the EMcam with the signal generator off and on, respectively.

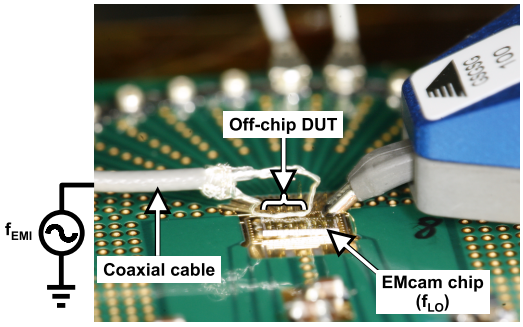

Fig. 10 Photograph of the measurement setup for the off-chip DUT.

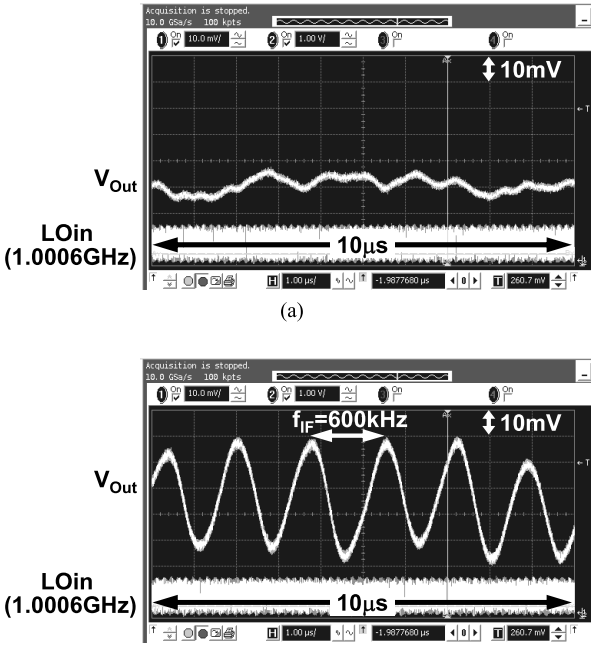

Fig. 11 Measured output waveforms of the EMcam with the signal generator (a) off and (b) on.

The frequencies of f_{EMI} and f_{LO} are 1 GHz and 1.0006 GHz, respectively. The frequency of, f_{IF} is 600 kHz. In Fig. 11(b), the output shows 600 kHz sinusoidal wave. This shows the off-chip EMI detection is successful and the EMcam measures not the power-supply noise but the off-chip EMI noise.

3.3 On-Chip DUT

In order to carry out stand-alone measurement of the EMcam chip, EMI noise emulators are also embedded on the same chip, namely on-chip DUT. Figures 12 (a) and (b) show schematics of the two DUTs for EMI noise emulation. In the DUT (wire), a long on-chip wire is driven by an off-chip signal generator to emulate arbitrary waveforms of EMI noise. The DUT (buffer) emulates clock buffers to emulate the global clock distribution in the logic circuits. Figure 13 shows the photograph of the measurement setup for the on-chip DUT. The EMI noise to be measured is fed

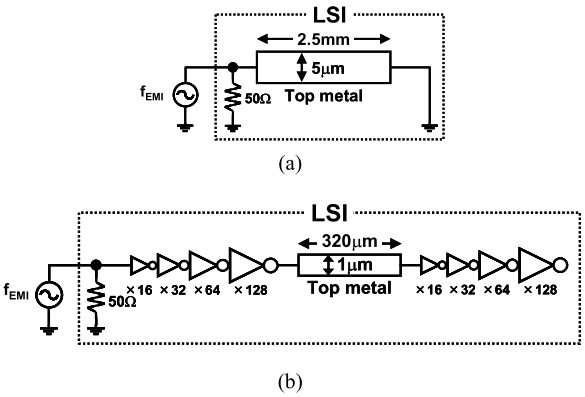

Fig. 12 On-chip DUTs for EMI noise generation. (a) DUT (wire). (b) DUT (buffer) (© 2010 IEEE).

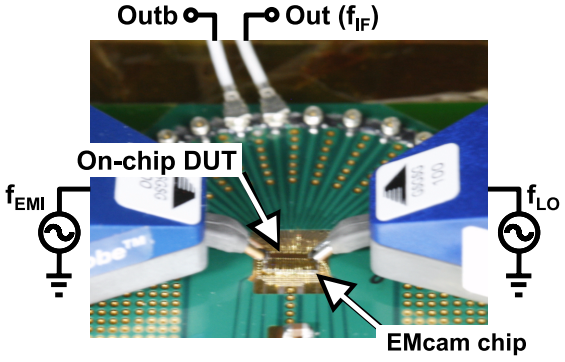

Fig. 13 Photograph of the measurement setup for the on-chip DUT.

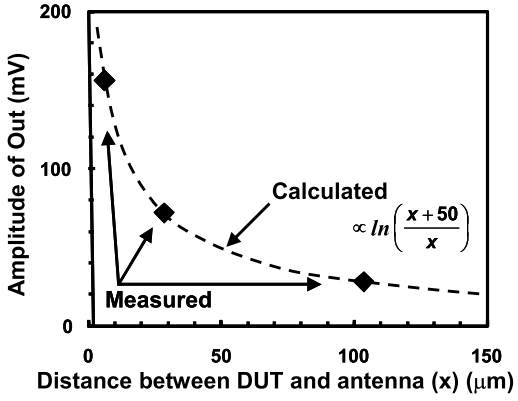

Fig. 14 Measured and calculated dependence of EMcam output on the distance between DUT (wire) and antenna (© 2010 IEEE).

by the external signal source, f_{EMI}. The external local oscillator, f_{LO} drives the mixer in the EMcam chip.

Figure 14 shows a measured and calculated dependence of the amplitude of the EMcam output on the distance between the DUT (wire) of 2 GHz sine and the antenna. The power input to the DUT by f_{EMI} is approximately 5 mW. In this measurement, the NCG is turned off and the noise inputs are not down-converted and directly measured without LPF. The following is a procedure of the calculated results in Fig. 14.

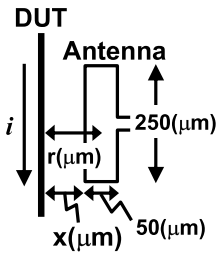

Fig. 15 Layout of the DUT (wire) and the antenna in Fig. 14.

In Fig. 15, the magnetic flux density B is described by

$$B = \frac{\mu_0}{2\pi} \cdot \frac{i}{r}, \tag{1}$$

where μ_0, r, and i are the magnetic permeability, the distance from the DUT, and the current in the DUT, respectively. And the magnetic flux Φ_m is calculated by using (1),

$$\begin{aligned}\Phi_m &= \oiint_S B \cdot dS = \frac{\mu_0}{2\pi} \cdot i \cdot c \int_x^{x+50} \frac{1}{r} dr \\ &= \frac{\mu_0}{2\pi} \cdot i \cdot c \cdot \ln\left(\frac{x+50}{x}\right),\end{aligned} \tag{2}$$

where

$$i = A \sin \omega t, \tag{3}$$

where A is the amplitude of the current. Therefore, the induced electromotive force $v(t)$ in the antenna is calculated by using (2) and (3),

$$v(t) = \frac{d\Phi_m(t)}{dt} = \mu_0 A f c (\cos \omega t) \ln\left(\frac{x+50}{x}\right), \tag{4}$$

where f is the frequency of the current. $v(t)$ is proportional to $\ln((x+50)/x)$. That means the EMcam output is proportional to the function $\ln((x+50)/x)$. In Fig. 14, the measured results agree with the calculated results, although there are some uncertainties such as A and x.

To check the operation of a mixer, an EMI measurement with the proposed down-conversion architecture is compared to that with the off-chip spectrum analyzer instead of the architecture. The EMI noise is emulated using the DUT (wire) and the off-chip 1 GHz signal generator. The f_{LO} sweeps from 15 MHz to 3.35 GHz at 2.7 MHz step. Each measurement point takes 24 seconds and the total time for 1192 measurement point, from 15 MHz to 3.35 GHz, is approximately 8 hours. To reduce the measurement time in practical use, number of measurement point should be optimized. Figure 16(a) shows measured EMI noise spectrum using the off-chip spectrum analyzer, when the NCG is turned off same as Fig. 14. Figure 16(b) shows corresponding EMI noise spectrum using the EMcam when the NCG is turned on. In Figs. 16(a) and (b), the noise peaks match at 1 GHz, 2 GHz, and 3 GHz. This confirms the operation of the mixer. On the other hand, the peak intensity ratios between 1, 2, and 3 GHz differ between Figs. 16(a) and 16(b). The differences are caused by the unity gain of the amplifier.

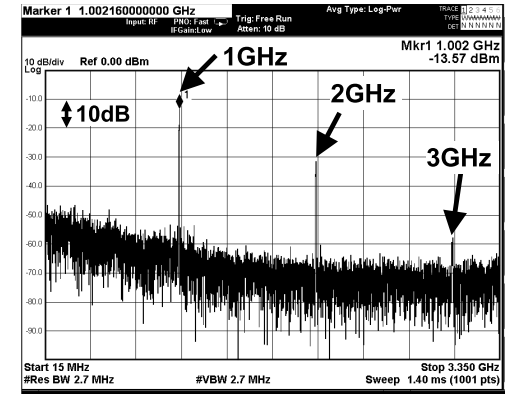

(a)

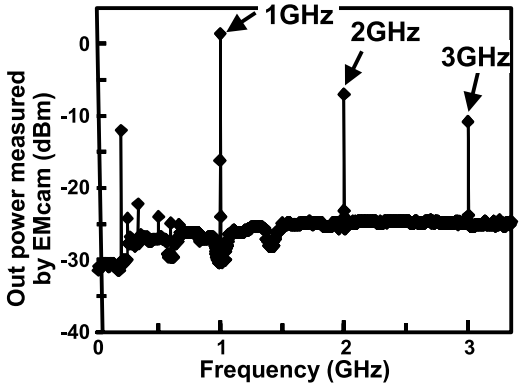

(b)

Fig. 16 EMI noise spectra with DUT (wire). (a) Spectrum for reference measured by external spectrum analyzer. (b) Spectrum measured by the EMcam chip.

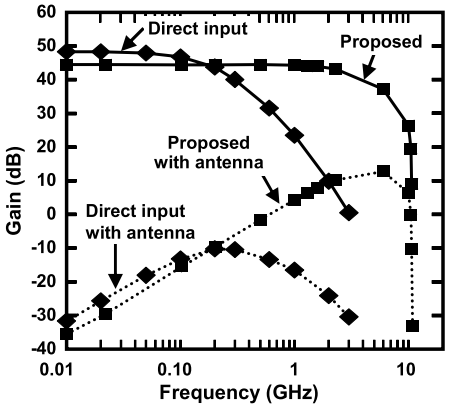

Fig. 17 Simulated frequency response of the measurement circuits with and without antenna.

Thanks to the down-conversion architecture, the proposed EMcam successfully measures the noise peak intensity up to 3.3 GHz while the noise peak intensity in Fig. 16(a) is attenuated.

Figure 17 shows the simulated frequency response of the measurement circuits (NCG, the Mixer, and the Amplifiers) in Fig. 3. Frequency responses including antenna characteristic of 20 dB/decade are also plotted. With the direct input, the unity gain frequency is 3 GHz. In contrast, with the proposed down-converted input (f_{IF}=2 MHz), the equivalent unity gain frequency is 11 GHz. The 3 GHz peak in Fig. 16(b) is higher than that in Fig. 16(a), which agrees with the bandwidth in Fig. 17.

Measurements with the EMI noise generated by the DUT (buffer) are carried out to emulate the clock buffer noise, which is the main EMI noise source in a digital LSI. Figures 18(a) and (b) show EMI noise waveform and spectrum of DUT (buffer) using the off-chip oscilloscope and spectrum analyzer, respectively, when V_{DD} of the DUT (buffer) is 1.2 V. The NCG is turned off, same as Fig. 14. In Fig. 18(a), the EMI noise waveform is clearly shown at the rising and falling edge of the 30 MHz clock signal. Figure 18(c) shows corresponding EMI noise spectrum using the EMcam when the NCG is turned on. In Figs. 18(b) and (c), the noise peaks match at 30 MHz and odd numbers of this. This confirms the validity of the EMcam. Figure 18(d) shows a measured dependence of the amplitude of the EMcam output on the power supply voltage of the DUT (buffer), when the NCG is turned on. The f_{LO} is 29.5 MHz. The amplitude is reduced with the reduced power supply voltage, because the EMI noise generation is reduced.

Figure 19 shows a within-die 2D distribution of EMI noise measured with the 12×4 on-chip loop antenna matrix of the EMcam. The antenna pitch is 260 μm and 60 μm in a horizontal and vertical direction, respectively. The DUT wire goes across the matrix. At this time f_{EMI} and f_{LO} are 1 GHz and 1.0006 GHz, respectively. As the distance between the DUT and the antenna increases, the measured EMI noise decreases.

In order to show the possibility of an EMcam with higher-spatial resolution, EMI measurement with the smallest size loop antenna ($32 \times 12\,\mu m^2$) is demonstrated. In this measurement, the NCG is turned off same as Fig. 15. Figure 20 shows a measured dependence of the amplitude of the EMcam output on the amplitude of the DUT (wire) input. As the input amplitude decreases, the output amplitude linearly decreases, which shows a reasonable operation of the smallest antenna. The performance is summarized in Table 1.

4. Conclusion

An EMI Camera LSI with a 12×4 on-chip loop antenna matrix in 65 nm CMOS is presented. The feasibility of the within-die 2D EMI distribution measurement with 60 μm-level spatial resolution is demonstrated without mechanical scanning. The down-conversion architecture and 'mixer and antenna selector (MAS)' are proposed to relax both the increase of power and area penalty, which are inherent issues of the matrix measurement. The down-conversion architecture increases the bandwidth of EMcam and enables the measurement of EMI spectrum. The shared IF block architecture reduced the power and the area by 74% and 73%, respectively. MAS reduces the switches and prevents the EMI attenuation due to the switches. EMI measurement with the

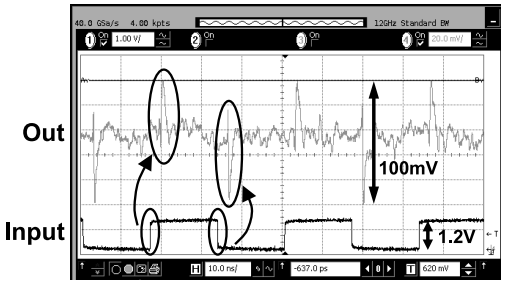

(a)

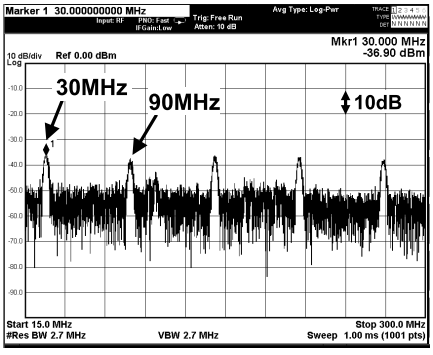

(b)

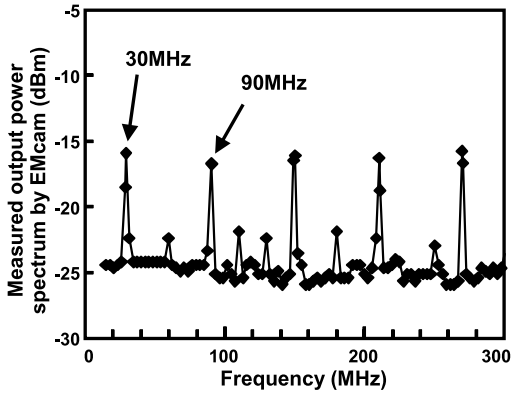

(c)

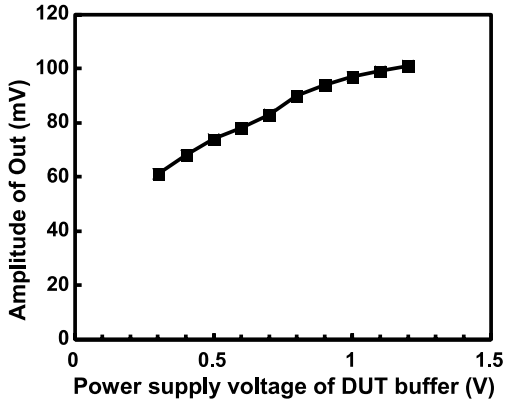

(d)

Fig. 18 EMI noise of DUT (buffer). (a) Noise waveform. (b) Noise spectrum for reference. (c) Noise spectrum using the EMcam. (d) Measured dependence of EMcam output on power supply voltage of DUT (© 2010 IEEE).

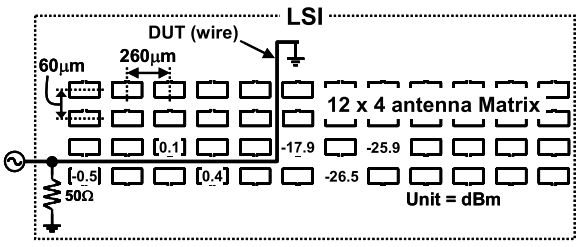

Fig. 19 Within-die 2D distribution of EMI noise measured with the 12×4 on-chip antenna matrix (© 2010 IEEE).

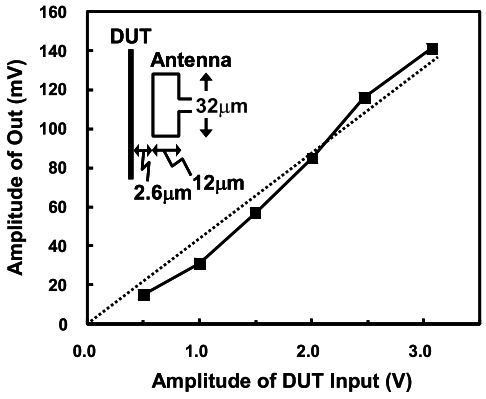

Fig. 20 Measured dependence of EMcam output on DUT (wire) input with the smallest antenna (© 2010 IEEE).

Table 1 Performance summary of the EMI camera LSI. (© 2010 IEEE)

Technology		65nm CMOS
Supply voltage		1.2V
EMI camera LSI	Gain	47dB
	Maximum frequency	3.3GHz
	Frequency resolution	3MHz
	Dynamic range	33dB
On-chip loop antenna	Number	12 x 4 array
	Size	250μm x 50μm (array) 32μm x 12μm (single)
	Antenna pitch	60μm (vertical) 260μm (horizontal)
Power	Amplifiers	16.06mW
	MAS and NCG	0.16mW
	Total	16.22mW
Core area	Amplifiers	2130μm^2
	MAS and NCG	46μm^2
	Total	2176μm^2

smallest antenna ($32 \times 12\,\mu m^2$) is also achieved. The measurement result with the smallest antenna demonstrates the feasibility of an EMI noise measurement with higher-spatial resolution in the future.

Acknowledgments

This work is partially supported by METI. The VLSI chips were fabricated through the chip fabrication program of VDEC in collaboration with STARC.

References

[1] M. Ramdani, E. Sicard, A. Boyer, S. Ben Dhia, J.J. Whalen, T.H. Hubing, M. Coenen, and O. Wada, "The electromagnetic compatibility of integrated circuits—Past, present, and future," IEEE Trans. Electromagn. Compat., vol.51, no.1, pp.78–100, Feb. 2009.
[2] Magnetic field probe (CP-1S), NEC Corporations.
[3] EMSCAN. [Online]. Available: http://emscan.com/
[4] K. Ishida, N. Masunaga, Z. Zhou, T. Yasufuku, T. Sekitani, U. Zschieschang, H. Klauk, M. Takamiya, T. Someya, and T. Sakurai, "Stretchable EMI measurement sheet with 8×8 coil array, 2 V organic CMOS decoder, and 0.18 μm silicon CMOS LSIs for electric and magnetic field detection," IEEE J. Solid-State Circuits, vol.45, no.1, pp.249–259, Jan. 2010.
[5] N. Masunaga, K. Ishida, Z. Zhou, T. Yasufuku, T. Sekitani, T. Someya, M. Takamiya, and T. Sakurai, "A flexible EMI measurement sheet to measure electric and magnetic fields separately with distributed antennas and LSI's," IEEE International Symposium on Electromagnetic Compatibility, pp.156–160, Austin, USA, Aug. 2009.
[6] N. Uddin and A. Thiede, "Switchable double-sensor integrated active probe for near-field scanner," Proc. 6th European Microwave Integrated Circuits Conference (EuMIC), pp.37–40, Oct. 2011.
[7] N. Ando, N. Masuda, N. Tarnaki, T. Kuriyama, S. Saito, K. Kato, K. Ohashi, M. Saito, and M. Yarnaguchi, "Miniaturized thin-film magnetic field probe with high spatial resolution for LSI chip measurement," IEEE International Symposium on Electromagnetic Compatibility, vol.2, pp.357–362, Santa Clara, USA, Aug. 2004.
[8] S. Aoyama, S. Kawahito, and M. Yamaguchi, "An active magnetic probe array for the multiple-point concurrent measurement of electromagnetic emissions," IEEE Trans. Magn., vol.42, no.10, pp.3303–3305, Oct. 2006.
[9] N. Masunaga, K. Ishida, M. Takamiya, and T. Sakurai, "EMI camera LSI (EMcam) with on-chip loop antenna matrix to measure EMI noise distribution with 60 μm-level spatial precision," IEEE Custom Integrated Circuits Conference (CICC), pp.449–452, San Jose, USA, Sept. 2010.

Naoki Masunaga received the B.S. and M.S. degrees in electronic engineering from Sophia University, Tokyo, Japan and University of Tokyo, Tokyo, Japan, in 2008 and 2010, respectively. His research interests are in the field of integrated circuit design. He is now with Terumo Corporation.

Koichi Ishida received the B.S. degree in electronics engineering from the University of Electro-Communications, Tokyo, Japan, in 1998, and received the M.S. and Ph.D. degrees in electronics engineering from the University of Tokyo, Tokyo, Japan, in 2002 and 2005, respectively. He joined Nippon Avionics Co., Ltd. Yokohama, Japan in 1989, where he developed high-reliability hybrid microcircuits for aerospace programs. Since July 2007, he has been working at Institute of Industrial Science, the University of Tokyo as a research associate. His research interests include low-voltage low-power CMOS analog circuits, on-chip power supply circuits, and large-area flexible electronics. He is a member of IEEE.

Takayasu Sakurai received the Ph.D. degree in EE from the University of Tokyo in 1981. In 1981 he joined Toshiba Corporation, where he designed CMOS DRAM, SRAM, RISC processors, DSPs, and SoC Solutions. He has worked extensively on interconnect delay and capacitance modeling known as Sakurai model and alpha power-law MOS model. From 1988 through 1990, he was a visiting researcher at the University of California Berkeley, where he conducted research in the field of VLSI CAD. From 1996, he has been a professor at the University of Tokyo, working on low-power high-speed VLSI, memory design, interconnects, ubiquitous electronics, organic IC's and large-area electronics. He has published more than 400 technical publications including 100 invited presentations and several books and filed more than 200 patents. He will be an executive committee chair for VLSI Symposia and a steering committee chair for IEEE A-SSCC from 2010. He served as a conference chair for the Symp. on VLSI Circuits, and ICICDT, a vice chair for ASPDAC, a TPC chair for the A-SSCC, and VLSI symp., an executive committee member for ISLPED and a program committee member for ISSCC, CICC, A-SSCC, DAC, ESSCIRC, ICCAD, ISLPED, and other international conferences. He is a recipient of 2010 IEEE Donald O. Pederson Award in Solid-State Circuits, 2010 IEEE Paul Rappaport award, 2010 IEICE Electronics Society award, 2009 achievement award of IEICE, 2005 IEEE ICICDT award, 2004 IEEE Takuo Sugano award and 2005 P&I patent of the year award and four product awards. He gave keynote speech at more than 50 conferences including ISSCC, ESSCIRC and ISLPED. He was an elected AdCom member for the IEEE Solid-State Circuits Society and an IEEE CAS and SSCS distinguished lecturer. He is a STARC Fellow and IEEE Fellow.

Makoto Takamiya received the B.S., M.S., and Ph.D. degrees in electronic engineering from the University of Tokyo, Japan, in 1995, 1997, and 2000, respectively. In 2000, he joined NEC Corporation, Japan, where he was engaged in the circuit design of high speed digital LSI's. In 2005, he joined University of Tokyo, Japan, where he is an associate professor of VLSI Design and Education Center. His research interests include the circuit design of the low-power RF circuits, the ultra low-voltage logic circuits, the low-voltage DC-DC converters, and the large area electronics with organic transistors. He is a member of the technical program committee for IEEE Symposium on VLSI Circuits. He received 2009 and 2010 IEEE Paul Rappaport Awards.